A LARGE-SIGNAL MODEL FOR THE PRC-LCC RESONANT TOPOLOGY WITH A CAPACITOR AS OUTPUT FILTER.

CIEP 2002
Guadalajara, MEXICO
October 20-24

Martín-Ramos J. A., Díaz J., Pernía A. M., Prieto M. J., Linera, F.F.
A.T.E. Universidad de Oviedo.
Ed. Departamentales Oeste. Módulo 3. Campus de Viesques s/n.
33204 Gijón. SPAIN.
e-mail: juan@ate.uniovi.es

Abstract: **In this paper, two mathematical models are presented to approximate, accurately enough, the large signal dynamical behaviour and the steady state behaviour of the PRC-LCC resonant topology with a capacitor as output filter. The method used to obtain these models is based on the applying of the extended describing function and the generalised averaging modelling techniques. Therefore, the evolution of the topology waveforms, most of them sinusoidal, is approximated by their corresponding envelope. These envelopes are expressed by a set of non linear differential equations which are solved numerically with the help of a computer. The resulting algorithm is faster than a straight PSpice simulation and free of convergence problems. Finally, the good concordance between the models and the practice is verified with a wide set of experimental results.**

I. INTRODUCTION.

The PRC-LCC with capacitive output filter (fig. 1) is a well-known topology, which has already been commented as available for high power applications [1]. In fact, as it combines the good behaviour of PRC at light load and SRC at full load, converters based on it are able to operate at a wide load range, being controlled by frequency and/or duty-cycle. Furthermore, considering its resonant stage arrangement, this topology appears as specially suitable for high-voltage applications, since the parasitic elements from the step up transformer are directly assumed by it [2], [4]. Nevertheless, its use as an effective solution has been ballasted because its complexity (more than two reactive components in its resonant stage) and the lack of simple models to aid the designer.

Certainly, a complete steady-state analysis has already been presented in some papers [3], [4], but its formulation is still complex. Also the small signal analysis with and LC output filter has been presented in [5], using the extended describing function concept. However, there has been no attempt in the literature addressing the large-signal modelling with a capacitor as output filter. This kind of filter, preferable for high voltage applications, presents additional complexity from the modelling point of view, since the output rectifier operates in discontinuous conduction mode, and therefore, the parallel capacitor, C_P, is regularly clamped to the value of the output voltage. Fig. 2 shows the main waveforms for this configuration.

In this paper, the different steps to obtain a large-signal model for this topology are presented. Moreover, also a simpler steady-state solution than in [3] is described, as and additional output. Both models are successfully contrasted with several experimental results, whose good agreement is also included.

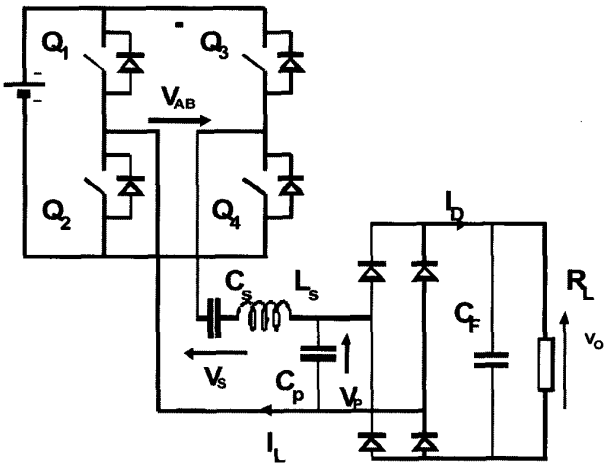

Figure 1.
PRC-LCC resonant topology with a capacitor as output filter.

II. NON-LINEAR STATE EQUATIONS. FIRST VERSION.

A simple analysis of the circuit in figure 2 allows to obtain a first expression for the non-linear state equations:

$$V_{AB}(t) = V_S(t) + V_P(t) + L_S \cdot \frac{di_L(t)}{dt} + r \cdot i_L(t) \qquad (1a)$$

$$C_S \cdot \frac{dV_S(t)}{dt} = i_L(t) \qquad (1b)$$

$$i_D = C_f \frac{dV_0(t)}{dt} + \frac{V_0}{R} \qquad (1c)$$

where "r " represents a series resistors with L_S in the resonant tank, quantifying the transformer and switching losses. The meaning of the other terms can be consulted in figure 1.

There are six variables: $V_S(t)$, $V_P(t)$, $V_0(t)$, $i_L(t)$, $i_D(t)$ and $V_{AB}(t)$, in three equations. Therefore, only three of these variables can remain. They are the three state variables which constitute the state vector [8], and are distinguished to be energy storing magnitudes. The other variables must be expressed as a function of the control parameters and the state variables.

On one hand, and paying attention to the energy storing magnitudes, the state vector is concluded to be composed by:

$$\bar{x}(t) = [i_L(t), V_S(t), V_0(t)\ ] \qquad (2)$$

On the other hand, the control variables (frequency, f, and duty cycle, d) are implicitly included in the input voltage to the resonant tank, V_{AB}.

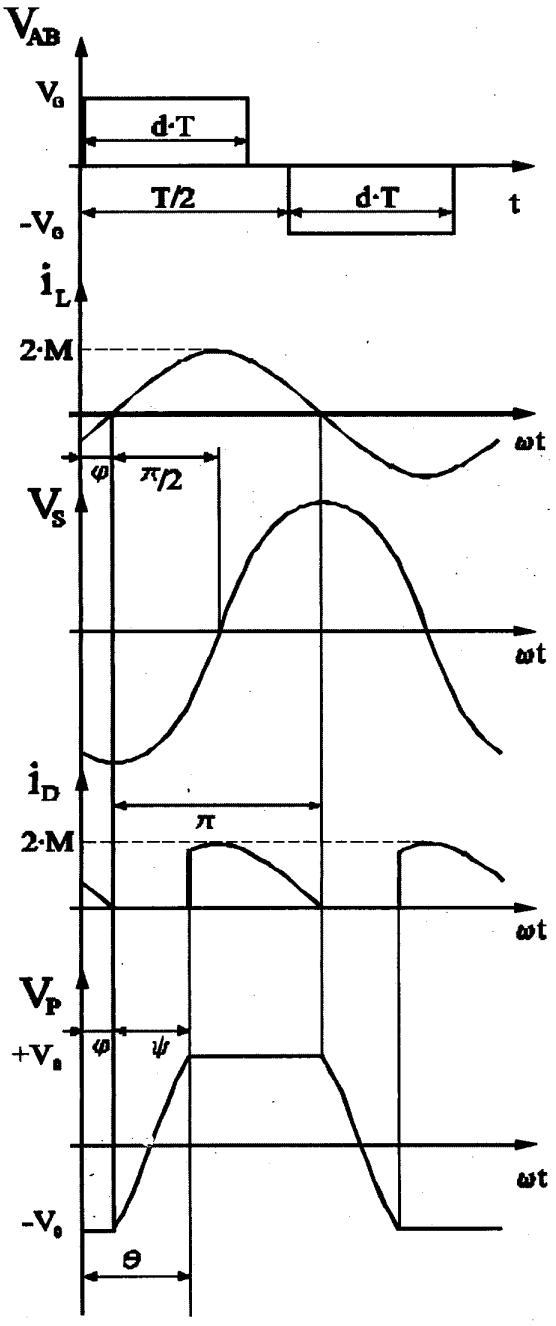

Figure 2.
Experimental main waveforms in a converter based on the PRC-LCC topology with a capacitor as output filter.

In short, the (1) expressions are not easy to evaluate, since there are too many variables and those related to the control are not present in an explicit way. Consequently, certain relationships must be found and, in the way, some simplifications will have to be done.

That the voltage in the parallel capacitor, V_P, has not been considered as state variable in (2), and that its differential relationship between current and voltage has not been included in (1), is remarkable. This is due to the fact that V_P waveform is not differentiable. In fact, V_P sinusoidal evolution is clamped to the output voltage, V_0, twice every period (fig 2), when the rectifying diodes are on. Then, the filter capacitor, C_f is connected in parallel with C_P. In comparison with C_f, C_P stores a very small amount of energy. The value of C_P is only relevant to establish, under any particular value of the resonant current, i_L, the time required for the sinusoidal transitions between the clamping values $+V_0$ and $-V_0$. Just considering the waveforms V_0 and i_L for every period is enough to calculate, dynamically, the appropriate value of • . Hence, the dynamic behaviour of V_P is completely defined by the energy stored in V_0 and i_L.

III. State Variables Harmonic Approach.

As figure 2 shows, the resonant current and the series capacitor voltage are predominantly sinusoidal, without any DC component and low presence of high frequency harmonics. Thus, it is accurate enough to approximate these magnitudes by their fundamental terms in the Fourier series. So, using the exponential formulation, the equalities (3) and (4) can be written:

$$i_L(t) \approx \langle i_L \rangle_1(t) \cdot e^{j\omega \cdot t} + \langle i_L \rangle_{-1}(t) \cdot e^{-j\omega \cdot t} \quad (3)$$

$$V_S(t) \approx \langle V_S \rangle_1(t) \cdot e^{j\omega \cdot t} + \langle V_S \rangle_{-1}(t) \cdot e^{-j\omega \cdot t} \quad (4)$$

being j the imaginary unit, • the pulsation and every $\langle y \rangle_k$ a complex Fourier coefficient whose value can be calculated as:

$$\langle y \rangle_k(t_0) = \frac{1}{T}\int_{t_0-T}^{t_0} y(\tau) e^{-k \cdot j\omega\tau} d\tau \quad (5)$$

where $\tau \in [t_0 - T, t_0]$. In the calculation of (5), it can be verified that the terms $\langle y \rangle_{-k}$ and $\langle y \rangle_k$ are complex conjugate. So, they can be expressed as:

$$\langle i_L \rangle_1 = x_1 + j \cdot x_2; \quad \langle i_L \rangle_{-1} = x_1 - j \cdot x_2 \quad (6a)$$

$$\langle V_S \rangle_1 = x_3 + j \cdot x_4; \quad \langle V_S \rangle_{-1} = x_3 - j \cdot x_4 \quad (6b)$$

being every x_i a real number.

Physically, x_1 and x_3 represent the semi-amplitudes of the cosenoidal part of i_L and V_S respectively. At the same time, x_2 and x_4 are the corresponding semi-amplitudes of the sinusoidal components. Therefore, the amplitude and phase of any of both waveforms can be easily evaluated. For instance:

$$M = \sqrt{x_1^2 + x_2^2} \quad (7a)$$

$$sin\varphi = \frac{-x_1}{\sqrt{x_1^2 + x_2^2}} \quad (7b)$$

On the other hand, the output voltage is a continuous magnitude and shows very low ripple. It can be approximated by its average value. By making this assumption:

$$V_O(t) = \langle V_0 \rangle_0(t) \quad (8a)$$

$$\langle V_0 \rangle_0(t) = x_7(t) \quad (8b)$$

Notice that terms into brackets and any x_i are time dependants, in consequence, their dynamic behaviour can be investigated. However, it must be remarked that their variation is slow when compared to the period length.

IV. EXTENDED DESCRIBING FUNCTION (E.D.F.)

To simplify the model stated in (1), and to obtain a useful one, it is necessary to express V_{AB}, V_P and i_D as a function of the control (f, d, V_G) and/or the state variables (x_1, x_2, x_3, x_4, x_7). The major hindrance for that, is the presence of two non-linear stages (inverter and output rectifier). The extended describing function concept, [6] [7], would have to be applied. This way, the equations for each stage will be re-written in a proper manner.

A. *Inverter stage.*

This stage generates a quasi-square voltage at its output, which is applied to the resonant tank (fig 1 & 2). The E.D.F. method is applied to obtain a Fourier formulation for this voltage as function of the control variables, since it only depends on d and V_G (fig 2). So, it can be written:

$$V_{AB}(t)=\sum_k f_{1k}(d,V_G)\cdot e^{j\omega\cdot t} \qquad (9)$$

where f_1 is the extended describing function for this stage, and f_{1i} is its i-esime harmonic component. As the resonant tank acts as a band-pass filter, the inverter must be tuned. In this situation, the effect of any harmonic component of V_{AB}, but the first, can be neglected (first harmonic prevalence). The sinusoidal appearance of the resonant current confirms this fact. Therefore, it is accurately enough to consider only the first harmonic for V_{AB}, and (9) transforms into (10):

$$V_{AB}(t)=f_{1,1}(d,V_G)\cdot e^{j\omega\cdot t}+f_{1,-1}(d,V_G)\cdot e^{-j\omega\cdot t} \qquad (10)$$

Attending to the information contained in fig. 2, (10) can be integrated, resulting (12.

$$f_{1,1}(d,V_G)=\frac{V_G}{\pi}\cdot[sin(2\pi d)-j+j\cdot\cos(2\pi d)] \qquad (11)$$

where $f_{1,-1}$ is the complex conjugate of $f_{1,1}$.

B. *Output rectifier stage.*

The E.D.F. method is applied to this stage to the obtain the describing functions, $f_2(t)$ and $f_3(t)$ for the voltage in the parallel capacitor, $V_P(t)$, and for the current through the rectifier diodes, $i_D(t)$. Both of them should depend on the state and the control variables.

To work out these functions, the behaviour of the stage must be investigated with the help of fig. 2. There, it can be observed that, when $V_P(t)$ is clamped to the output voltage, the resonant current goes through the rectifying diodes and $i_D(t)=i_L(t)$. Then, $i_L(t)$ changes its sign and all the diodes are off. The current $i_L(t)$ flows entirely through C_P, and its voltage experiments a sinusoidal evolution from $-V_0$ to $+V_0$ (or vice versa), being clamped again. With this clamping, all this process is repeated. Hence, it can be affirmed that the conduction periods in the output rectifier bridge are determined exclusively by two of the state variables, $V_0(t)$ and $i_L(t)$.

With this, (12) can be written:

$$V_P(t)=\sum_k f_{2,k}(i_L,V_0)\cdot e^{j\omega\cdot t} \qquad (12a)$$

$$i_D(t)=\sum_k f_{3,k}(i_L,V_0)\cdot e^{j\omega\cdot t} \qquad (12b)$$

Again, the resonant tank band-pass filtering action explains the prevalence of the first harmonic effects on $V_P(t)$. On the contrary, the output filter has been design to provide DC voltage, and only the average value of $i_D(t)$ is relevant for this magnitude (fig 3). Hence, (14a) and (14b) can be easily admitted.

$$V_P(t)=f_{2,1}(i_L,V_0)\cdot e^{j\omega\cdot t}+f_{2,-1}(i_L,V_0)\cdot e^{-j\omega\cdot t} \qquad (13a)$$

$$i_D(t)=f_{3,0}(i_L,V_0) \qquad (13b)$$

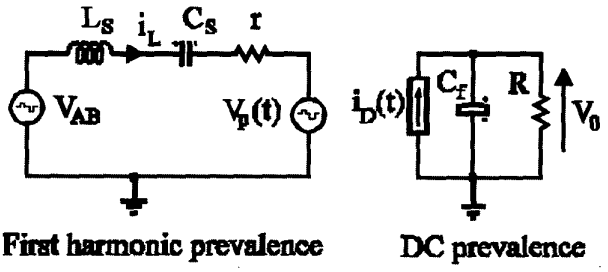

Figure 3.
Simplified equivalent circuit for the topology. The state variables appearance is sinusoidal in the net on the right and continuous on the left.

If the values of $i_L(t)$ and $V_0(t)$ are known, the angle • can be calculated from the sinusoidal transition of $V_P(t)$. Bearing in mind C_P initial and final voltage, and that the transition occurs when the whole resonant current goes through it, expression (14b) is easily deduced from (14a).

$$V_P(\theta)=V_P(\varphi)+\frac{1}{C_P}\cdot\int_\varphi^\theta i_L(t)\cdot d\omega t \Rightarrow \qquad (14a)$$

$$\cos\psi=1-\frac{x_7\cdot C_P\cdot\omega}{\sqrt{x_1^2+x_2^2}} \qquad (14b)$$

Bearing in mind all the aforementioned data about $V_P(t)$ and $i_D(t)$, the following expressions about $V_P(t)$ are obtained:

$$f_{2,1}=x_5+j\cdot x_6;\quad f_{2,-1}=x_5-j\cdot x_6 \qquad (15a)$$

$$x_5=\frac{1}{\pi\cdot C_P\omega}\left[x_1\cdot sin^2\psi+x_2\cdot\mu\right] \qquad (15b)$$

$$x_6=\frac{1}{\pi\cdot C_P\omega}\left[x_2\cdot sin^2\psi-x_1\cdot\mu\right] \qquad (15c)$$

where:

$$\mu=[\psi-sin\psi\cdot\cos\psi] \qquad (15d)$$

and about $i_D(t)$:

$$f_{3,0}(i_L,V_0)=\frac{2\cdot\sqrt{x_1^2+x_2^2}}{\pi}\cdot[1+\cos\psi] \qquad (15e)$$

V. HARMONIC BALANCE.

In (1), the state variables appear also in their first derivative form. In order to simplify the system, they must also be approximated by their corresponding harmonic term. Assuming frequency as a time invariant magnitude, or at least with a slowly enough variation:

$$\frac{d(i_L(t))}{dt}=\frac{d}{dt}\left[\langle i_L\rangle_1\cdot e^{j\cdot\omega t}+\langle i_L\rangle_{-1}\cdot e^{-j\cdot\omega t}\right]= \tag{16a}$$
$$\left[\frac{d\left[\langle i_L\rangle_1\right]}{dt}+j\omega\langle i_L\rangle_1\right]\cdot e^{j\cdot\omega t}+\left[\frac{d\left[\langle i_L\rangle_{-1}\right]}{dt}-j\omega\langle i_L\rangle_{-1}\right]\cdot e^{-j\cdot\omega t}$$

and identically:

$$\frac{dV_S(t)}{dt}=\left[\frac{d\left[\langle V_S\rangle_1\right]}{dt}+j\omega\langle V_S\rangle_1\right]\cdot e^{j\cdot\omega t} \tag{16b}$$
$$+\left[\frac{d\left[\langle V_S\rangle_{-1}\right]}{dt}-j\omega\langle V_S\rangle_{-1}\right]\cdot e^{-j\cdot\omega t}$$

$$\frac{dV_O}{dt}=\frac{d\langle V_0\rangle_0}{dt} \tag{16c}$$

Now, it is possible to re-write (1), using the results obtained in the harmonic approximation of Section III, and the E.D.F. of Section IV. In all the resulting equations, the exponential terms $e^{j\omega\cdot t}$ and $e^{-j\omega\cdot t}$ can be put into separated groups, and, this way, every equation is divided into two complex conjugated ones. Now there are two complex-conjugated systems whose solutions are complex-conjugated. Therefore, taking into account one of them is enough, being possible to simplify (1) to:

$$L_S\frac{d\left[\langle i_L\rangle_1\right]}{dt}=f_{1,1}-\langle V_S\rangle_1-f_{2,1}-(jL_S\omega+r)\langle i_L\rangle_1 \tag{17a}$$

$$C_S\cdot\frac{d}{dt}\left[\langle V_S\rangle_1\right]=\langle i_L\rangle_1+j\omega\cdot\langle V_S\rangle_1 \tag{17b}$$

$$C_f\frac{d\langle V_0\rangle_0}{dt}=f_{3,0}(i_L,V_0)-\frac{\langle V_0\rangle_0}{R} \tag{17c}$$

where the new state vector will be:

$$\bar{x}(t)=\left[\langle i_L\rangle_1(t),\langle V_S\rangle_1(t),\langle V_0\rangle_0(t)\right] \tag{18}$$

Equations (17a) and (17b) are complex. To separate them in real and imaginary parts is a good idea. Remembering (6), (8b) and (14) and substituting the E.D.F. expressions, (17) becomes:

$$L_S\frac{dx_2}{dt}=\frac{V_G}{\pi}\left[\cos(2\pi d)-1\right]-x_4-x_6-rx_2-\omega L_S x_1 \tag{19a}$$

$$L_S\cdot\frac{dx_1}{dt}=\frac{V_G}{\pi}\cdot sin(2\pi d)-x_3-x_5-rx_1+\omega L_S x_2 \tag{19b}$$

$$C_S\cdot\frac{dx_3}{dt}=x_1+\omega C_S\cdot x_4 \tag{19c}$$

$$C_S\cdot\frac{dx_4}{dt}=x_2-\omega C_S\cdot x_3 \tag{19d}$$

$$C_f\cdot\frac{dx_7}{dt}=-\frac{x_7}{R}+\frac{2\cdot\sqrt{x_1^2+x_2^2}}{\pi}\cdot[1+\cos\psi] \tag{19e}$$

The system is completed with (14b) and (15d). In this situation, the new state vector will be :

$$\bar{x}(t)=[x_1,x_2,x_3,x_4,x_7] \tag{20}$$

where the state variables are the complex coefficients of the Fourier exponential series.

The differential equations system (19) constitutes a large signal model by itself. To obtain a solution, it is just necessary to integrate it. Numerical methods are used with this purpose, and a software package has been developed for P.C., based on the Runge Kutta module 4 integrating method. The predictions calculated this way have been compared successfully with experimental measurements and Pspice simulations, Section VIII.

VI. Steady State Equations

Any large signal model contains, implicitly, an steady state solution. To obtain it the derivatives in (19) are substituted by zero, since the variables does not experiment any change in steady state. The solution of the remaining system is showed in (21).

$$\psi_0=Arc\ \cos\left(\frac{\pi-2R\cdot C_P\cdot\omega_0}{\pi+2R\cdot C_P\cdot\omega_0}\right) \tag{21a}$$

being $0\le\psi_0\le\pi$.

$$\mu_0=[\psi_0-\text{sen}\psi_0\cdot\cos\psi_0] \tag{21b}$$

$$g_0=\left[1+\pi\cdot r\cdot C_P\cdot\omega_0-\cos^2\psi_0\right] \tag{21c}$$

$$H_0=\frac{C_S\cdot g_0}{\pi\cdot C_P+\mu_0\cdot C_S-\pi\cdot\omega_0^2\cdot L_S\cdot C_S\cdot C_P} \tag{21d}$$

$$x_{20}=\frac{H_0^2}{1+H_0^2}\frac{C_P\cdot\omega_0\cdot V_{G0}}{g_0}\cdot\left(\frac{sin(2\pi\cdot d_0)}{H_0}+\right. \tag{21e}$$
$$\left.+\cos(2\pi\cdot d_0)-1\right)$$

$$x_{10}=\frac{-x_{20}}{H_0}+\frac{C_P\cdot\omega_0\cdot V_{G0}}{g_0}\cdot sin(2\pi\cdot d_0) \tag{21f}$$

$$x_{30}=\frac{x_{20}}{C_S\cdot\omega_0} \tag{21g}$$

$$x_{40}=\frac{-x_{10}}{C_S\cdot\omega_0} \tag{21h}$$

$$x_{50}=\frac{1}{\pi\cdot\omega_0\cdot C_P}\left[x_{10}\cdot\text{sen}^2\psi_0+x_{20}\cdot\mu_0\right] \tag{21i}$$

$$x_{60}=\frac{1}{\pi\cdot\omega_0\cdot C_P}\left[x_{20}\cdot\text{sen}^2\psi_0-x_{10}\cdot\mu_0\right] \tag{21j}$$

$$x_{70}=\frac{4R}{\pi+2R\cdot\omega_0\cdot C_P}\sqrt{x_{10}^2+x_{20}^2} \tag{21k}$$

where the subindex '0' means steady state magnitude.

With this model, it is very simple to collect in graphics the operation points of any converter. These graphics can adopt several formats depending on the magnitudes studied and on which of them are maintained constant. In the figures 4 and 5 some graphics are presented as an example. In them, all the magnitudes have been normalised according to the base in the annexe, and C_S has been kept equal to C_P.

VII. Optimum Switching Line.

To drive this topology into the optimum switching line can result interesting from the converter losses point of view [4]. In this mode of operation, no energy is returned from the resonant circuit to the input voltage source (minimising processed energy and conduction losses) and the four switches are forced off (minimising switching losses). To work under this condition it is necessary to maintain null the phase between the resonant current and the inverter output voltage, $\bullet=0$. Therefore, resonant current should be sensed,

and a feedback loop should be implemented to synchronise the switching of one leg of the inverter with the resonant current zero-crossing. The duty cycle is determined this way, using its value to assure right synchronisation. The appearance of the resulting topology waveforms is very similar to that described in fig 2, but $\varphi = 0$.

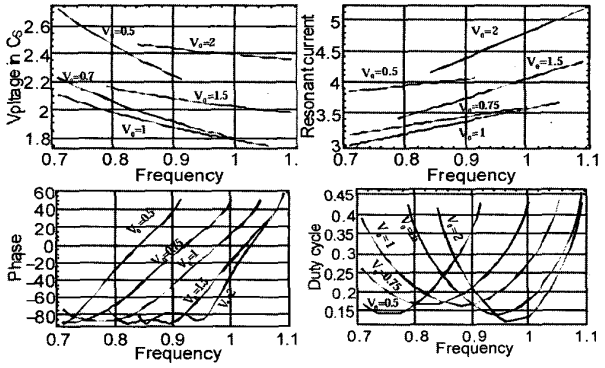

Figure 4.

- Steady state relationships, when the output power is 1 per unit and the output voltage, V_0, is changing. All the magnitudes are normalised.

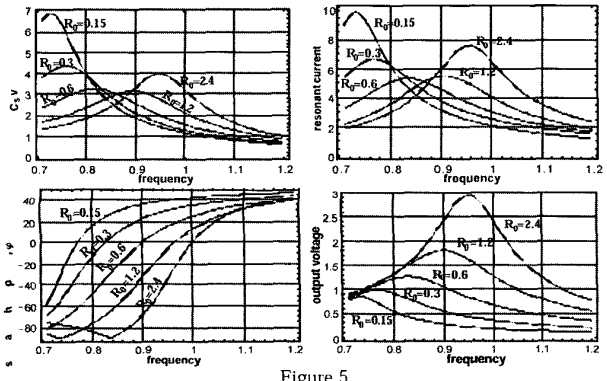

Figure 5

- Steady state relationships for different constant loads, when the duty cycle is constant: d_0=0.3. All magnitudes are normalised.

Considering Section VII, it is very simple to model this operation mode in steady state. It is just necessary to oblige x_{10}, cosenoidal component of $i_L(t)$, to be null in system (21). The required duty cycle to maintain this value can be calculated from (21e) and (21f), resulting :

$$d_0 = \frac{1}{p} \cdot Arctg[-H_0] \qquad (22)$$

and the rest of the system remains the same as in (21).

Now, it is possible to obtain some graphics from the model, in order to characterise the behaviour of the topology under these circumstances, fig. 6. Again, all the magnitudes have been normalised according to the base in the annexe, and C_S has been kept equal to C_P.

However, other relationships between capacities are possible, and the reaction of the converter also can be estimated under this circumstances. It is even possible to compare how the operation points are modified this way. In fig. 7, there is an example of this possibility. The magnitudes at this figure has been normalised with the base in the annexe, considering:

$$a = \frac{C_S}{C_S + C_P} \qquad (2)$$

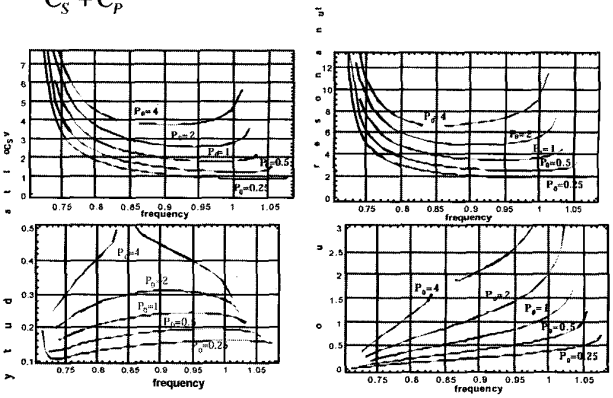

Figure 6

Steady state relationships for different output power situations, under optimum switching line condition. All magnitudes are normalised.

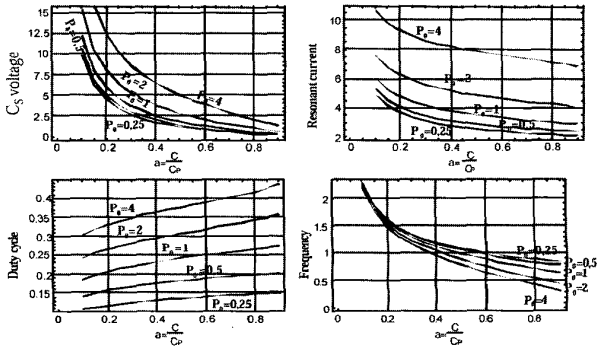

Figure 7

Steady state curves for different constant power transferred to the output, when the output voltage is 1 p. u., the relationship between the resonant capacities, a, changes and the optimum switching line mode of operation is observed.

VIII. Experimental Results.

A. *Large Signal Model.*

The numerical solution of the large signal model provides, as result, the dynamical evolution of all the magnitudes in the converter. Notwithstanding, the accuracy in some of them is very difficult to check. For instance, it is easy to represent the modelled evolution of $q(t)$ and $\varphi(t)$, but not the experimental ones. In fig. 7 theoretical (envelope) and experimental results for the state variables are shown, with high agreement grade, during an input voltage step in the conditions of table 3.

TABLE 3

f	d	V_G	R
75,76 kHz	0,4	0V TO 36.8V	24,5W

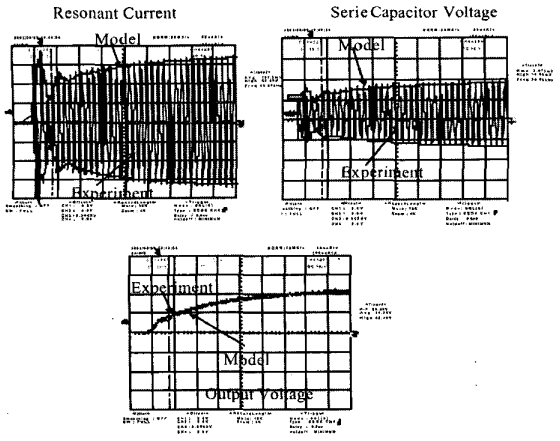

Figure 7.

Experimental and modelled evolution for the states variables under conditions in table 3.

B. Steady State Solution.

In table 2, a set of experimental values are compared with theoretical for permanent conditions. An excellent agreement between them must be remarked. Also the few calculus time required.

TABLE 2.
EXPERIMENT VS. MODEL STEADY STATE VALUES

	f_0	d_0	V_{G0}	R	φ_0	I_L^{MAX}	θ_0	V_S^{MAX}	V_0
Prototype	65.36 KHz	0.276	39.2 V	80 •	-99.3°	8.4 A	43.4°	94 V	78.4 V
Model	65.36 KHz	0.276	39.2 V	80 •	-81.5°	9.9 A	51.4°	94.9 V	80.9 V
Error	-	-	-	-	17.8°	17.9%	8°	1%	3.2%
Prototype	70.9 KHz	0.112	20 V	11.1 •	-33.6°	1.68 A	57.7°	15.2 V	6.4 V
Model	70.9 KHz	0.112	20 V	11.1 •	-20.7°	1.8 A	62.6°	16 V	7.2 V
Error	-	-	-	-	12.9°	7.1%	4.9°	5.3%	12.5%
Prototype	71.43 KHz	0.44	36 V	45 •	-5.4°	17.4 A	115.5°	170 V	131.7 V
Model	71.43 KHz	0.44	36 V	45 •	-13.5°	18.6 A	108.4°	163.9 V	125.4 V
Error	-	-	-	-	8.1°	6.9%	7.1°	3.6%	4.8%
Prototype	75.76 KHz	0.284	36.8 V	24.5 •	7.2°.	8.4 A	115.2°	68.8 V	45.6 V
Model	75.76 KHz	0.284	36.8 V	24.5 •	11.6°	8.3 A	119.2°	68.8 V	45.4 V
Error	-	-	-	-	4.2°	1.2%	4°	0%	0.4%
Prototype	82 KHz	0.217	37.6 V	66.7 •	23.5°	6.05 A	141.7°	54.4 V	46.3 V
Model	82 KHz	0.217	37.6 V	66.7 •	17.8°	6.7 A	151.5°	50.8 V	43.6 V
Error	-	-	-	-	5.7°	10.7%	9.8°	6.6%	5.8%
Prototype	89.29 KHz	0.335	39.2V	66.7 •	50.2°	5.68 A	184.2°	45.6 V	39.5 V
Model	89.29 KHz	0.335	39.2V	66.7 •	48.5°	6 A	184°	42.3 V	36.8 V
Error	-	-	-	-	1.7°	5.6%	0.2°	7.2%	6.8%
Avg. error	-	-	-	-	8.4°	8.2%	5.7°	4%	5.6%

The data required for calculations are on white boxes.

IX. CONCLUSIONS

A very simple steady state model and a large signal model have been deduced for the PRC-LCC topology with a capacitor as output filter. The models predict with an excellent precision and really low calculus time all the electrical circuit magnitudes, using harmonic approach and extended description functions. Furthermore, their accuracy has been confirmed by experimentation.

X. REFERENCES:

[1] Robert L. Steigerwald " A comparision of half-bridge resonant converter topologies" IEEE Transaction on industrial Electronics, Vol. 3 N° 2 April 1988

[2] J.M. Sun, S.P. Wang, T. Nishimura and M. Nakaoka " Resonant Mode PWM DC-DC Converter with a high-voltage transformer link and its control methods for medical-use X-ray power supply" EPE'99 Lausanne

[3] V. García, M. Rico, J. Sebastián, M Hernando "Using the Hybrid Series Parallel Resonant Converter with Capacitive Output Filter and PWM Phase-Shifted Control for High- Voltage Applications". IEEE IECON'94 pages 1659-1664

[4] V. García, M. Rico, J. Sebastián, M Hernando and J. Uceda. "An Optimized DC-DC Converter Topology for High Voltage Pulse Loads Applications" IEEE PESC 94 pages 1413-1421.

[5] Eric X. Yang, Fred Lee and Milan M. Jovanovic " Small-Signal modeling of LCC resonant converter "PESC 1992 pages 941-948

[6] E.X. Yang F.C. Lee and M.M. Jovanovic " Extended Describing function Technique applied to the modelling of resonant converters" VPEC 1991

[7] E.X. Yang F.C. Lee and M.M. Jovanovic " Small-signal modelling of power electronic circuits using extended describing function technique " VPEC 1991

[8] S. R. Sanders, J. M. Noworolski, X. Z. Liu, G. Verghese. "Generalized Averaging Method for Power Conversion Circuits." IEEE Trans. on Power Electronics, Vol. 6, n°2, pp. 251-259, April 1991.

[9] J. Martin-Ramos, J. Diaz, A. M. Pernía, F. Nuño, J. Sebastián. "A Large Signal Model for the PRC-LCC topology witha a Capacitor as Output Filter". APEC 2002 pp- 1120-1126.

XI. ANNEXE.

Base of normalization:

Voltage: $V_B = V_G$

Impedance: $Z_B = \sqrt{\frac{L_S}{C}}$

Frequency: $f_B = \frac{1}{2\pi\sqrt{L_S \cdot C}}$

where C is the series association of C_S and C_P:
From previous base magnitudes, any other can be defined.

This work has been supported by CICYT.